International Journal of Physics and Applications

E-ISSN: 2664-7583
P-ISSN: 2664-7575
IJOS 2024; 6(1): 08-14

www.physicsjournal.in
Received: 23-11-2023
Accepted: 24-12-2023

Yuvraj Ruparel
Aditya Birla World Academy, Vastu Shilp, JD Road Annexe, Gamadia Colony, Tardeo, Mumbai, Maharashtra, India

Corresponding Author:
Yuvraj Ruparel
Aditya Birla World Academy, Vastu Shilp, JD Road Annexe, Gamadia Colony, Tardeo, Mumbai, Maharashtra, India

Synthesis of a Ni- BCA/CF hybrid composite for high-performance lithium-ion battery anode

Yuvraj Ruparel

DOI: https://doi.org/10.33545/26647575.2024.v6.i1a.78

Abstract
The growing need for high-performance lithium-ion batteries (LIBs) has sparked research into novel anode materials, leading to the development of a hybrid composite material with improved electrochemical performance. This study presents a novel composite material consisting of nickel (Ni) and benzene-1, 4-dicarboxylic acid (BCA) incorporated into carbon fibers (CF), focusing on enhancing synergistic interactions. The intricate manufacturing process enables an even distribution of Ni-BCA nanoparticles on the CF substrate. SEM, XRD, and FTIR are used for evaluating structural and morphological characteristics. The interconnected network of nickel-borate coated aluminum nanoplates enables consistent charge distribution, leading to improved electrochemical performance. An electrochemical study of Ni-BCA/CF as a sole electrode material indicates a significant specific capacitance of 784 mAh g^{-1} with a current density of 0.1 $A.g^{-1}$. Trasatti investigation, using cyclic voltammetry to examine charge distribution, showed that including CF enhances the charge storage capacity of the hybrid composite. The findings unveil a distinctive hybrid composite for high-performance LIBs and provide crucial insights for designing and synthesizing improved anode materials to address current energy storage challenges.

Keywords: Lithium-ion battery, metal organic framework, 4, 4'-biphenyl dicarboxylic acid, carbon nanofibers, anode

Introduction
The increasing need for high-performance lithium-ion batteries (LIBs) has prompted extensive research into advanced anode materials in order to meet the growing energy storage demands of modern society. The current increase in research focused on porous organic coordination networks represents a fundamental change in the field of energy storage architecture. This evolutionary process, facilitated by the complex self-assembly of links (Ligands) and connectors (Metals), involves a network that is stabilized by the interactions between metals and ligands. It signifies a significant departure from the engineering of carefully crafted cavities within coordination networks.

The foundation of this design paradigm can be identified in the landmark finding of the Hofmann complex by Hofmann and Kuspert in 1897. This discovery established the way for highly structured materials that have the capacity to bring about a paradigm shift in the field of energy storage. A turning point occurred in 1995 when Yaghi and his colleagues introduced Metal-Organic Frameworks (MOFs). With their unprecedented structural diversity and tunability, MOFs ushered in a new era of polynuclear metal carboxylate complexes by combining the advantageous properties of organic and inorganic components. MOFs have become a subject of significant interest in scientific research due to their extensive range of applications, which includes catalysis, gas separation, drug delivery, chemical sensing, and most notably, energy storage systems, with batteries being the most prominent example. Notwithstanding their extensive applicability and unique attributes, the inherent constraints of MOFs have instigated diligent endeavors to rectify these difficulties and fully exploit their capabilities. Our research is centered around the synthesis of Nickel (Ni) Metal-Organic Frameworks (MOFs) through the innovative utilization of Benzene-1, 4-dicarboxylic acid (BCA). This approach aims to overcome the limitations that are typically associated with traditional MOFs. The synthesis method places a high value on cost-effectiveness through the utilization of a room temperature mixing technique with solutions of organic linkers and metal salts in water [7-9].

This emphasizes our dedication to environmental sustainability as we avoid the use of hazardous organic solvents and reduce reliance on costly equipment.

The resultant Ni-BCA demonstrates a distinctive morphology distinguished by nanoplates that are continuously interconnected, which has significant ramifications for its electrochemical capabilities. Detailed characterization investigations uncover the considerable pore size and surface area of Ni-BCA, which establish it as a formidable contender for anodes with enhanced performance in lithium-ion batteries. The objective of the development of a new composite material, Ni-BCA/CF, is to improve electrochemical performance by combining physical and chemical charge storage mechanisms in a synergistic manner [10-12]. This will ultimately enhance the anode material's capabilities. Through a thorough examination of the electrochemical characteristics of Ni-BCA/CF using a solitary electrode in a 6M KOH electrolyte, we have identified an exceptionally high specific capacitance and exceptional cycle stability. The implications of these results for novel approaches to energy storage are encouraging.

2. Experimental

2.1 Synthesis of Ni-BPDC/CF

All chemicals utilized in the present study were of analytical reagent (AR) grade and employed as received without further purification. The synthesis of Nickel Metal-Organic Frameworks (Ni MOFs) was conducted using the ligand Benzene-1, 4-dicarboxylic acid (BCA) following a previously reported method [23]. In a typical synthesis, an aqueous solution of the organic ligand was prepared by dissolving 4.75 x 10-3 mol of BPDC in 100 mL distilled water (DW). The pH of this solution was adjusted to 7 using 1 M NaOH. Simultaneously, the metal ion solution was prepared by dissolving 3.72 x 10-3 mol of Nickel chloride in 100 mL DW. The freshly prepared metal ion solution was then slowly added dropwise into the organic ligand solution, and the resulting mixture was stirred at room temperature for 12 hours. A green-colored precipitate formed over time, indicating the successful formation of Ni MOFs. The synthesized Ni MOFs were subsequently filtered, washed successively with DW and ethanol, and then dried at 60 °C for 24 hours. Subsequently, in the synthesis of the composite material, 50 mg of Carbon Nanofibers (CNF) were introduced to the Ni MOF solution, and the mixture was sonicated for approximately 30 minutes to ensure thorough and uniform mixing [14].

2.2. Material Characterization

X-ray Diffraction (XRD) patterns of the synthesized materials were recorded using a Shimadzu 7000S X-ray diffractometer equipped with CuKα radiation (λ=0.154 nm). The measurements were conducted in the range of 5 to 70° to ascertain the crystallographic structure.

Fourier Transform Infrared (FTIR) spectra were acquired using a Shimadzu-8400S spectrometer, covering the frequency range of 4000 cm^{-1} to 400 cm^{-1}. This analysis provided insights into the molecular vibrations and functional groups present in the synthesized materials. Thermo Gravimetric Analysis (TGA) was performed utilizing a Perkin-Elmer thermal analyzer. The analysis covered a temperature range from room temperature to 1000 °C, employing an alumina reference crucible. The heating rate was maintained at 10 °C/min, offering valuable information on the thermal stability and decomposition characteristics. The Brunauer-Emmett-Teller (BET) specific surface area and pore dimensions of Ni MOFs were determined through N_2 adsorption-desorption measurements at 77 K. This analysis provided crucial information about the material's porosity and surface characteristics. Surface morphology analysis was conducted using Field Emission Scanning Electron Microscopy (FESEM) on an FEI INSPECT F50 instrument. Additionally, Energy-Dispersive X-ray Spectroscopy (EDX) was employed to analyze the elemental composition of the materials. These techniques collectively provided a comprehensive understanding of the structural, thermal, and morphological attributes of the synthesized material.

2.3 Electrochemical characterization in three electrode system

The cyclic voltammetry (CV) experiments were conducted within a voltage window of 0 to 3.0 V at various scan rates, while galvanostatic charge-discharge (GCD) studies were carried out in a similar voltage range but at different current densities. Electrochemical Impedance Spectroscopy (EIS) studies were also performed to comprehensively analyze the electrochemical behavior. For the assessment of Ni-BCA/CF as anode materials for lithium-ion batteries (LIBs), coin cells were employed to measure battery performance. The preparation involved mixing as-prepared powders of Ni-BCA/CF (80 wt%), acetylene carbon black (10 wt%), and polyvinylidene fluoride (PVDF) binder (10 wt%) in N-methyl-2-pyrrolidone (NMP) to form a slurry [15-17]. This slurry was then coated onto a copper current collector, dried at 80 °C under vacuum overnight, roll-pressed, and cut into disks with a diameter of 10 mm. The force exerted on the foil during roll-pressing was approximately 10 MPa for two minutes, resulting in an active material loading content of about 1.7 mg/cm². The coin cells were assembled in an argon-filled glove box with oxygen and water content maintained below 1 ppm. Lithium foil served as the counter and reference electrode, and a 1.0 M LiPF6 electrolyte dissolved in ethylene carbonate (EC) and diethyl carbonate (DEC) (in a volume ratio of 1:1) was utilized. Celgard 2400 film served as the separator. After assembly, the cells were left undisturbed for 12 hours before electrochemical tests were performed. Subsequently, the cells were disassembled in the argon-filled glove box, and the electrodes were washed with DEC. The pole piece was then sent for testing in a vacuum box [18-20].

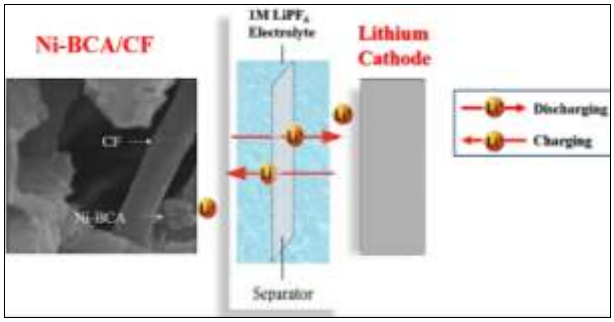

Fig 1: Schematic illustration for Ni- BCA /CF hybrid composite Anode material and lithium foil as a cathode in 1M $LiPF_6$ electrolyte.

3. Results and Discussions

Structural characterization of synthesized materials

The XRD patterns of Ni-BCA/CF are illustrated in Fig. 2 (D), where CF exhibits its characteristic high-intensity peak at 27° associated with the (002) crystal plane [27]. In the case of Ni-BCA displays peaks at 5.5°, 11.1°, 13.1°, 15.2°, 18.6°, and 20.4°. These peaks observed in the case of Ni-BCA are also

present in the XRD pattern of Ni-BCA/CF but with lesser intensity. This suggests that the introduction of CNF does not disrupt the linkages between the metal centre and organic ligand. However, due to weak electrostatic interaction between Ni-BPDC and CNF, the intensity of diffraction peaks assigned to Ni-BPDC is slightly reduced in the composite. Furthermore, the peak observed in the CNF aligns with the peak at around 26° in the Ni-BPDC, confirming the crystalline nature of the Ni MOFs and verifying the successful formation of the Ni-BPDC/CNF composite [22-26].

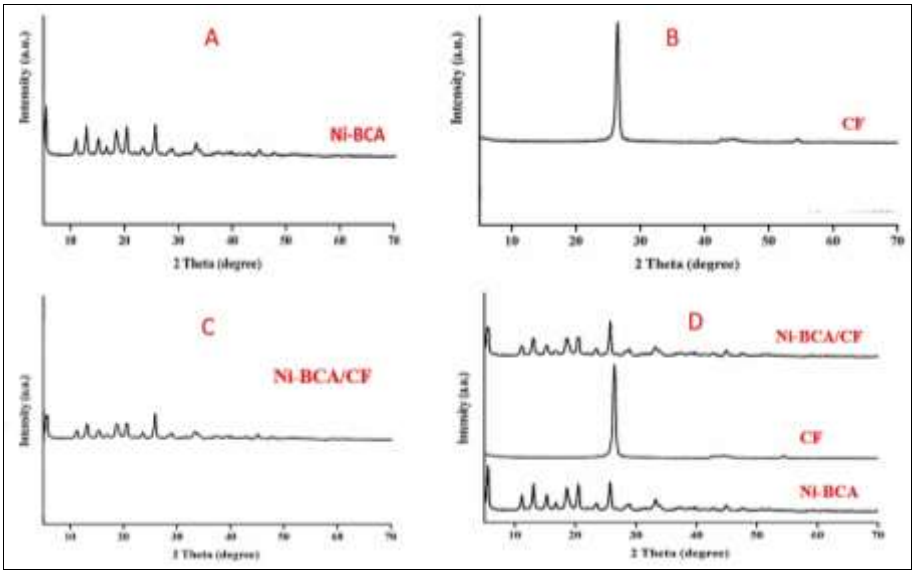

Fig 2: XRD patterns of as synthesized materials

The confirmation of Ni-BCA/CF composite formation was further substantiated through FTIR spectroscopy. In Fig. 3, the FTIR spectra of Ni-BPDC reveal two intense bands at 681 $cm^{-1}$and 705 cm^{-1}, indicating the presence of the C-H antiplane bending mode of the aromatic ring [28]. The band at 1600 cm^{-1}signifies the C=C stretching mode, confirming the presence of the aromatic ring [29]. Four bands at 852 cm^{-1}, 1393 cm^{-1}, 1539 cm^{-1}, and 1587 cm^{-1}correspond to the stretching mode of carboxylate groups (COO-) coordinated to the metal center [26]. Specifically, the bands at 1393 $cm^{-1}$and 1587 $cm^{-1}$are attributed to the symmetric and asymmetric stretching modes of COO- groups, suggesting coordination through a bidentate mode [30, 31]. Additionally, bands at 3300 $cm^{-1}$and 3600 cm^{-1} indicate –OH vibrations from water molecules present in the MOF structure [26]. The FTIR spectra of Ni-BCA/CF (Fig. 3, B) show additional peaks in the higher frequency region compared to pristine Ni-BCA. The peak at 2980 cm^{-1} is assigned to the stretching mode of the methylene (–CH2) group, and the broad peak around 3430 cm^{-1}corresponds to –OH stretching mode due to the presence of functional groups on the CF surface [32]. The FTIR analysis for structure elucidation confirms the successful formation of Ni-BCA/CF.

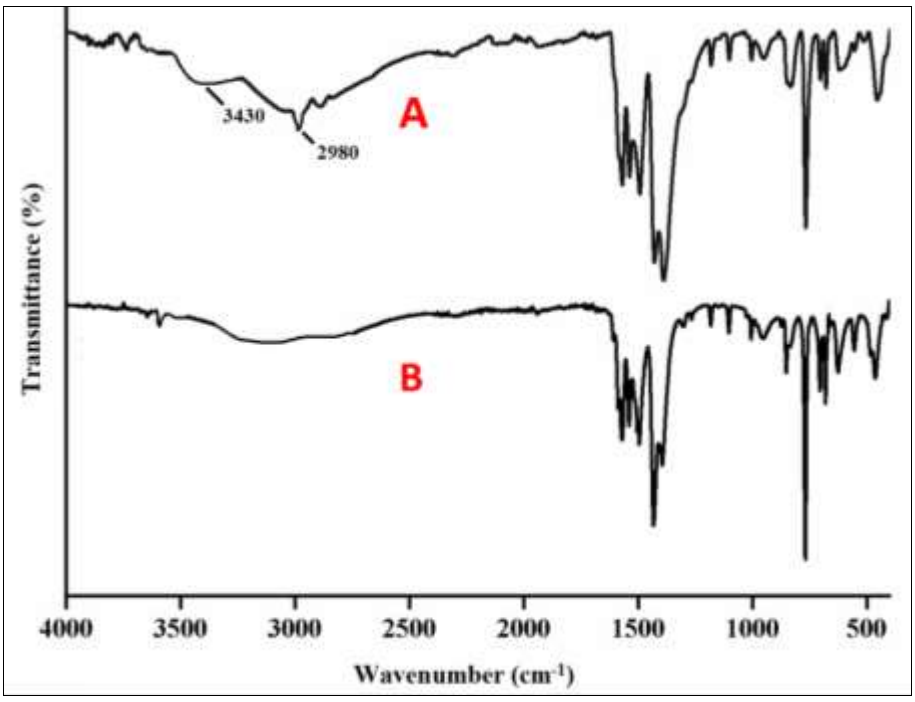

Fig 3: FTIR spectra of as synthesized materials

TGA studies were conducted to assess the thermal stability of the Ni-BCA/CF composite, and the TGA curve is depicted in Fig. 4. The initial weight loss observed in all four samples up to 300 °C is attributed to the removal of solvated water molecules from the MOF structure. Subsequently, the weight loss between 350 °C to 600 °C indicates the decomposition of Ni MOF into Nickel oxide [29, 33]. The % residues at 1000 °C were found to be 30.2% in the case of Ni-BCA/CF, further confirming the higher thermal stability of the composite.

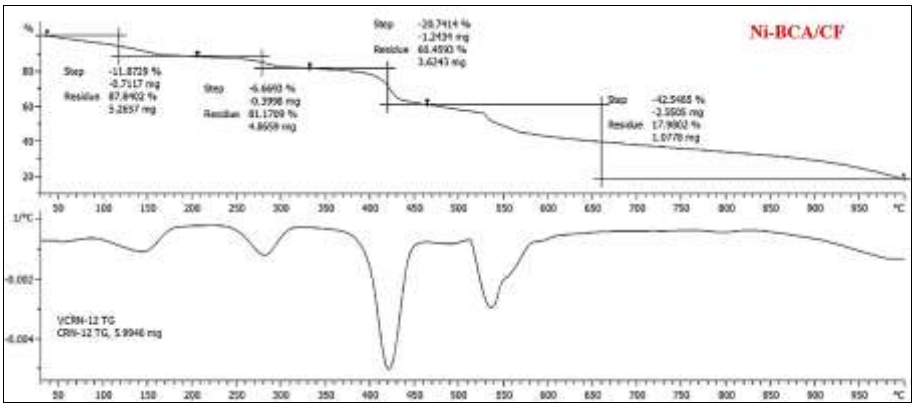

Fig 4: TGA studies to assess the thermal stability of the Ni-BCA/CF composite

The FESEM image of Ni-BCA/CF, as depicted in Fig. 5, provides a detailed view showcasing the presence of nanoplates of Ni-BPDC intricately linked to the surface of CNF (Fig-5 A). This visual evidence solidifies the confirmation of the successful formation of the composite, demonstrating a well-integrated structure where the Ni-BPDC nanoplates are effectively connected to the CNF framework. Further insight into the elemental composition was obtained through the EDX spectra of Ni-BCA/CF, as illustrated in Fig. 5 B. The spectra exhibit prominent peaks corresponding to the elements Ni, C, and O, verifying the formation of pristine Ni MOF and its retention in the composite structure. Notably, the weight percentage of carbon (C) in Ni-BPDC is measured at 36.3%, while in Ni-BCA/CF, this percentage increases to 49.2%. This substantial increase in the carbon content confirms the successful incorporation of carbon nanofibers (CF) into the framework of Ni-BCA, highlighting the enhanced structural complexity achieved in the composite material.

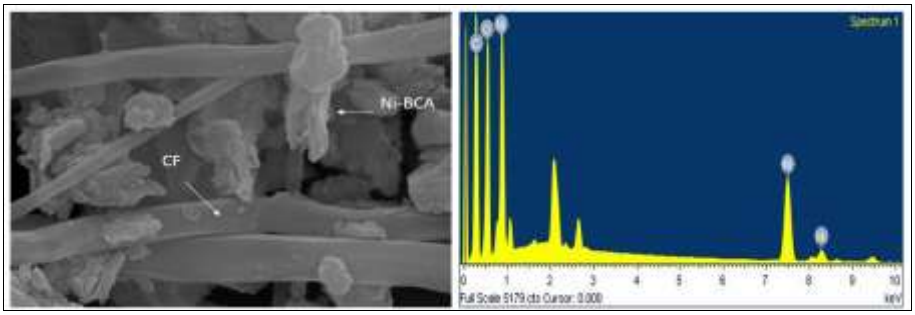

Fig 5: SEM and EDS to assess the morphology of Ni-BCA/CF composite

The introduction of carbon fibers (CF) has played a pivotal role in enhancing both the electrical conductivity and cyclic performance of Ni-BCA. To validate the impact of this modification by CF on the properties of Ni-BCA, a comprehensive set of electrochemical studies including cyclic voltammetry (CV), galvanostatic charge-discharge (GCD), and electrochemical impedance spectroscopy (EIS) were conducted using a three-electrode system [34-36].

In Fig. 7 (A), the CV curves of Ni-BCA/CF at a scan rate of 50 mV.s^{-1} and In Fig. 5, the galvanostatic charge-discharge profile for Ni-BCA/CF is presented within the voltage range of 0.0 to 3.0 V (vs. Li/Li+) at a current density of 0.1 A g^{-1}. The specific capacity values for the charging and discharging cycles are recorded as 784 mA g^{-1} and 761 mA g^{-1}, respectively. However, these values decrease to 520 mA g^{-1} for charging and 563 mA g^{-1} for discharging after 20 cycles. It is noted that the capacity contribution above 0.5 V mainly arises from Li adsorption at the defect sites and pores present in Ni-BCA. Despite the good electrical conductivity of CF sheets, the junction resistance between neighbouring sheets remains substantial, especially for randomly and loosely stacked sheets. The electrochemical performance of Ni-BCA/CF is further evaluated at higher current density values, reaching up to 2.0 A g^{-1}, as depicted in Fig. 5. The specific capacity values for charging and discharging cycles at this elevated current density are measured as 320 mA g^{-1} and 329 mA g^{-1}, respectively. The experimental results highlight a trend where reversible capacity is higher at lower current density values and vice versa. To assess the cyclic stability of Ni-BCA/CF, initial charging/discharging is conducted at 0.1 A g^{-1} for 20 cycles. Subsequently, the current rate is incrementally increased up to 2.0 A g^{-1}, maintaining 20 cycles at each rate (Fig. 5)[37-38]. Notably, the observed results demonstrate the material's remarkable capacity retention and stability even at high current rates, emphasizing its potential for robust performance in practical applications. In Figure 5d, electrochemical impedance spectroscopy (EIS) studies were undertaken at ambient temperature to gain deeper insights into the factors contributing to the improved electrochemical performance and stability of the Ni-BCA/CF composite. The

impedance spectra reveal distinctive features that elucidate the underlying electrochemical processes. At high frequencies, the intercept at the real axis (Z') is influenced by ohmic resistance, encompassing electrical connections, separator, and electrolyte resistance (Rs). The high-frequency semicircle is associated with Li+ ion transport through the solid-electrolyte interface (SEI) layer [39]. Meanwhile, the low-frequency semicircle arises from the constant phase element and charge transfer resistance (Rct) of the electrode/electrolyte interface. The subsequent nearly linear region in the graph signifies the diffusion of Li-ions into the electrode, represented as Warburg impedance. From the Nyquist plot, it is evident that the values of Rs and Rct for Ni-BCA/CF are determined to be 3.01 Ω and 35.11 Ω, respectively. These findings contribute to a comprehensive understanding of the impedance characteristics and highlight the improved electrical properties of the Ni-BCA/CF composite, showcasing its potential for advanced electrochemical applications.

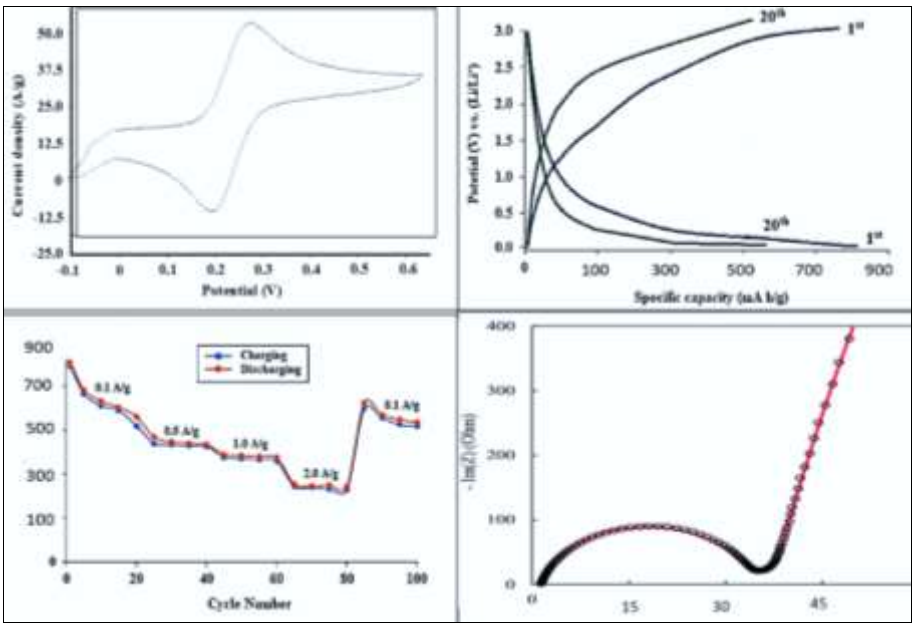

Fig 6: Electrochemical performance of Ni-BCA/CF composite anode material against lithium cathode in 1M $Lipf_6$ electrolyte.

Conclusions

In conclusion, this study has explored the synthesis and characterization of Ni metal organic frameworks (Ni MOFs) with benzene-1, 4-dicarboxylic acid (BPDC) as the organic ligand, with the aim of addressing the growing demand for high-performance lithium-ion batteries (LIBs). The synthesis methodology employed a cost-effective approach, involving room-temperature mixing of metal salt and organic linker solutions in water, bypassing the use of hazardous organic solvents and expensive instruments. The resulting Ni-BPDC exhibited a distinct morphology of continuously interconnected nanoplates, showcasing remarkable attributes of large pore dimensions and surface area, translating to superior electrochemical performance. To further augment the electrochemical capabilities, a composite material, Ni-BPDC/CNF, was introduced by incorporating carbon nanofibers (CNF). This composite demonstrated a synergistic combination of physical and chemical charge storage mechanisms, enhancing the overall performance of the anode material. Electrochemical characterization studies, including cyclic voltammetry (CV), galvanostatic charge-discharge (GCD) and electrochemical impedance spectroscopy (EIS), were conducted to evaluate specific capacitance, cyclic stability, and impedance characteristics. Specific charging and discharging capacities for Ni-BPDC/CNF were found to be 784 mAh g^{-1} and 761 mAh g^{-1}, respectively. Up to 100 cycles, the material demonstrated a specific capacity of 568 mAh g-1 at 0.1 A g-1. Furthermore, despite the high current density of 2 A g-1, a reversible capacity of 355 mAh g-1 was maintained after 65 cycles. These results highlight the robust cyclic stability and superior performance of Ni-BPDC/CNF, indicating its potential for practical applications in high-performance lithium-ion batteries. The study not only contributes a novel Ni-based MOF with nanoplate morphology but also underscores the broader implications of MOF-based composites in advancing the field of energy storage, particularly in the realm of high-performance lithium-ion battery anodes. The tailor-made synthesis approach and the insights gained from electrochemical studies pave the way for future research in the development of efficient and sustainable energy storage materials.

References

1. Simon P, Gogotsi Y. Materials for electrochemical capacitors. Nat Mater. 2008;7:845-854.
2. Chen PC, Shen G, Shi Y, Chen H, Zhou C. Preparation and characterization of flexible asymmetric super capacitors based on transition-metal-oxide nanowire/single-walled carbon nanotube hybrid thin-film electrodes. ACS Nano. 2010;4:4403-4411.
3. E-Kady MF, Strong V, Dubin S, Kaner RB. Laser scribing of high-performance and flexible graphene-based electrochemical capacitors. Science. 2012;335:1326-1330.
4. Bousquet CMI, Casteel WJ, Pearlstein RM, Girish Kumar G, Pez GP, Gomez-Romero P, *et al*. Polyfluorinated boron cluster – [B12F11H]2-based electrolytes for supercapacitors: Overcharge protection. Electrochem Commun. 2010;12:636-639.
5. Long JW, Belanger D, Brousse T, Sugimoto W, Sassin MB, Crosnier O. Asymmetric electrochemical capacitors stretching the limits of aqueous electrolytes. MRS Bull. 2011;36:513-522.
6. Umeshbabu E, Rajeshkhanna G, Rao GR. Effect of

solvents on the morphology of NiCo2O4/graphene nanostructures for electrochemical pseudocapacitor application. J Solid State Electrochem. 2016;20:1837-1844.
7. Liu T, Zhang F, Song Y, Li Y. Recent progress in layered double hydroxide based materials for electrochemical capacitors: Design, synthesis and performance. J Mater Chem A. 2017;5:17705-17733.
8. Zhao M, Zhao Q, Li B, Xue H, Pang H, Chen C. Revitalizing carbon supercapacitor electrodes with hierarchical porous structures. Nanoscale. 2017;9:15206-15225.
9. Ramya R, Sivasubramanian R, Sangaranarayanan MV. Conducting polymers-based electrochemical supercapacitors-Progress and prospects. Electrochim Acta. 2013;101:109-129.
10. Kostopoulou E, Kymakis E, Stratakis E. Perovskite nanostructures for photovoltaic and energy storage devices. J Mater Chem A. 2018;6:9765-9798.
11. Guo P, Huang X, Zhu X, Lü Z, Zhou Y. A new composite material Ca3Co4O9+δ +La0.7Sr0.3CoO3 developed for intermediate-temperature SOFC cathode. Fuel Cells. 2013;13:666-672.
12. Hu J, Shi L, Liu Q, Huang H, Jiao T. Improved oxygen reduction activity on silver-modified LaMnO3-graphene via shortens the conduction path of adsorbed oxygen. RSC Adv. 2015;5:92096-92106.
13. Javed MS, Raza R, Ahsan Z, Rafique MS, Shahzadi S, Shaukat SF, *et al*. Electrochemical studies of perovskite cathode material for direct natural gas fuel cell. Int J Hydrog Energy. 2016;41:3072-3078.
14. Jeon NJ, Noh JH, Yang WS, Kim YC, Ryu S, Seo J, *et al*. Solvent engineering for high performance inorganic-organic hybrid perovskite solar cells. Nature. 2015;517:476-480.
15. Suntivich J, Gasteiger HA, Yabuuchi N, Nakanishi H, Goodenough JB, Shao-Horn Y. Design principles for oxygen-reduction activity on perovskite oxide catalysts for fuel cells and metal-air batteries. Nat Chem. 2011;3:546-550.
16. Mefford JT, Hardin WG, Dai S, Johnston KP, Stevenson KJ. Anion charge storage through oxygen intercalation in LaMnO3 perovskite pseudocapacitor electrodes. Nat Mater. 2014;13:726-732.
17. Kalinin SV, Borisevich A, Fong D. Beyond condensed matter physics on the nanoscale: the role of ionic and electrochemical phenomena in the physical functionalities of oxide materials. ACS Nano. 2012;6:10423-10437.
18. George G, Jackson SL, Luo CQ, Fang D, Luo D, Hu D, *et al*. Effect of doping on the performance of high-crystalline SrMnO3 perovskite nanofibers as a supercapacitor electrode. Ceram Int. 2018;44:21982-21992.
19. Caruntu D, Rostamzadeh T, Costanzo T, Parizi SS, Caruntu G. Solvothermal synthesis and controlled self assembly of monodisperse titanium-based perovskite colloidal nanocrystals. Nanoscale. 2015;7:12955-12969.
20. Chen C, Wei Y, Jiao X, Chen D. Hydrothermal synthesis of BaTiO3: Crystal phase and the Ba2+ ions leaching behavior in aqueous medium. Mater Chem Phys. 2008;110:186-191.
21. Wang Y, Cui J, Yuan Q, Niu Y, Bai Y, Wang H. Significantly enhanced breakdown strength and energy density in sandwich-structured barium titanate/ poly (Vinylidene fluoride) nanocomposites. Adv Mater. 2015;27:6658-6663.
22. Parizi SS, Mellinger A, Caruntu G. Ferroelectric barium titanate nanocubes as capacitive building blocks for energy storage applications. ACS Appl Mater Interfaces. 2014;6:17506-17517.
23. Liu Y, Dinh J, Tad MO, Shao Z. Design of perovskite oxides as anion-intercalation-type electrodes for supercapacitors: cation leaching effect. ACS Appl Mater Interfaces. 2016;8:23774-23783.
24. Paraknowitsch JP, Thomas A. Doping carbons beyond nitrogen: an overview of advanced heteroatom doped carbons with boron, sulphur and phosphorus for energy applications. Energy Environ Sci. 2013;6:2839-2855.
25. Wang X, Sun G, Routh P, Kim DH, Huang W, Chen P. Heteroatom-doped graphene materials: syntheses, properties and applications. Chem Soc Rev. 2014;43:7067-7098.
26. Chen C, Wei Y, Jiao X, Chen D. Hydrothermal synthesis of BaTiO3: Crystal phase and the Ba2+ ions leaching behavior in aqueous medium. Mater Chem Phys. 2008;110:186-191.
27. Kalambate PK, Rawool CR, Srivastava AK. Voltammetric determination of pyrazinamide at graphene-zinc oxide nanocomposite modified carbon paste electrode employing differential pulse voltammetry. Sens Actuators B. 2016;237:196-205.
28. Gao H, Li Z, Qin X. Synthesis of carbon microspheres loaded with manganese oxide as air cathode in alkaline media. J Power Sources. 2014;248:565-569.
29. Chen N, Zhou J, Zhu G, Kang Q, Ji H, Zhang Y, *et al*. High-performance asymmetric supercapacitor based on vanadyl phosphate/carbon nanocomposite and polypyrrole-derived carbon nanowire. Nanoscale. 2018;10:3709-3719.
30. Li Z, Zhang W, Wang H, Yang B. Two-dimensional perovskite LaNiO3 nanosheets with hierarchical porous structure for high-rate capacitive energy storage. Electrochim Acta. 2017;258:561-570.
31. Pandolfo G, Hollenkamp AF. Carbon properties and their role in supercapacitors. J Power Sources. 2006;157:11-27.
32. Rawool R, Karna SP, Srivastava AK. Enhancing the supercapacitive performance of nickel based metal organic framework-carbon nanofibers composite by changing the ligands. Electrochim Acta. 2019;294:345-356.
33. Dang F, Kato K, Imai H, Wada S, Haneda H, Kuwabara M. A new effect of ultrasonication on the formation of BaTiO3 nanoparticles. Ultrason Sonochem. 2010;17:310-314.
34. Joshi UA, Lee JS. Template free hydrothermal synthesis of single-crystalline barium titanate and strontium titanate nanowires. Small. 2005;1:1172-1176.
35. Wen Y, Wang B, Huang C, Wang L, Jurcakova DH. Synthesis of phosphorus-doped graphene and its wide potential window in aqueous supercapacitors. Chem Eur J. 2015;21:80-85.
36. Utara S, Hunpratub S. Ultrasonic assisted synthesis of BaTiO3 nanoparticles at 25 °C and atmospheric pressure. Ultrason Sonochem. 2018;41:441-448.
37. Classen T, Lingenfelder M, Wang Y, Chopra R, Virojanadara C, Starke U, *et al*. Hydrogen and coordination bonding supramolecular structures of trimesic acid on Cu (110). J Phys Chem A.

2007;111:12589-12603.
38. Karthika P, Rajalakshmi N, Dhathathreyan KS. Phosphorus-doped exfoliated graphene for supercapacitor electrodes. J Nanosci Nanotechnol. 2013;13:1746-1751.
39. Chen P, Zhang Y, Zhao F, Gao H, Chen X, An Z. Facile microwave synthesis and photocatalytic activity of monodispersed BaTiO3 nanocuboids. Mater Character. 2016;114:243-253.